Application of synchrotron-radiation-based x-ray microprobe techniques for the analysis of recombination activity of metals precipitated at Si/SiGe misfit dislocations



2002 J. Phys.: Condens. Matter 14 13079

(http://iopscience.iop.org/0953-8984/14/48/353)

INSTITUTE OF PHYSICS PUBLISHING JOURNAL OF PHYSICS: CONDENSED MATTER

J. Phys.: Condens. Matter **14** (2002) 13079–13086 PII: S0953-8984(02)54062-5

# Application of synchrotron-radiation-based x-ray microprobe techniques for the analysis of recombination activity of metals precipitated at Si/SiGe misfit dislocations

**O F Vyvenko[1,3], T Buonassisi[1], A A Istratov[1], E R Weber[1], M Kittler[2] and W Seifert[2]**

[1] University of California, LBNL, 1 Cyclotron Rd, Berkeley, CA 94720, USA
[2] IHP, Im Technologiepark 25, D-15236 Frankfurt (Oder), Germany

E-mail: vyvenko@paloma.spbu.ru

Received 27 September 2002
Published 22 November 2002
Online at stacks.iop.org/JPhysCM/14/13079

**Abstract**

In this study we report application of synchrotron-radiation-based x-ray microprobe techniques (the x-ray-beam-induced current (XBIC) and x-ray fluorescence ($\mu$-XRF) methods) to the analysis of the recombination activity and space distribution of copper and iron in the vicinity of dislocations in silicon/silicon–germanium structures. A combination of these two techniques enables one to study the chemical nature of the defects and impurities and their recombination activity *in situ* and to map metal clusters with a micron-scale resolution. XRF analysis revealed that copper formed clearly distinguishable precipitates along the misfit dislocations. A proportional dependence between the XBIC contrast and the number of copper atoms in the precipitates was established. In hydrogen-passivated iron-contaminated samples we observed clusters of iron precipitates which had no recombination activity detectable by the XBIC technique as well as iron clusters which were not completely passivated.

## 1. Introduction

Transition metals are more detrimental to silicon device yield than any other impurity [1, 2]. Due to their high diffusivity and solubility in silicon, they easily penetrate from the wafer surface into the bulk during any heat treatment. The strong temperature dependence of the equilibrium solubilities of the metals causes their supersaturation during cooling, which results in the formation of metal precipitates or complexes. These precipitates are usually found in

[3] On leave of absence from: The Institute of Physics, St Petersburg State University, Russia.

  

the vicinity of structural defects such as grain boundaries or dislocations. Metal precipitates often form band-like states near the middle of the band gap [3–5], thus providing an effective channel for minority carrier recombination. Additionally, these precipitates may be charged. This can provide an attractive electrostatic potential for minority charge carriers and increase the effective minority carrier capture cross-section of the precipitates by orders of magnitude [5, 6].

In order to develop a quantitative model describing the recombination activity of metal precipitates, one has to have data on both recombination activity and the size of individual precipitates or groups of similar precipitates. Until recently, the only tool which was used to assess *in situ* the recombination activity and chemical nature of the precipitates was electron-beam-induced current (EBIC) combined with the energy-dispersive spectroscopy (EDS) mode of scanning electron microscopy (SEM). However, the detection limit of EDS was too low, about 0.1–1 at.%.

The use of the synchrotron radiation instead of a conventional x-ray tube allows increase of the sensitivity of the x-ray fluorescence ($\mu$-XRF) and absorption techniques, such that they can be used to characterize small metal clusters in silicon. It was shown [7] that the experimental facility of the beamline 10.3.1 of the Advanced Light Source at the Lawrence Berkeley National Laboratory allows detection of iron and copper in silicon with a 1–2 $\mu$m resolution in concentrations that are at least two orders of magnitude lower than the detection limit of the EDS–SEM technique. In the past, the samples used for XRF analysis were usually pre-characterized using EBIC or laser-beam-induced current (LBIC) in order to find the areas of low minority carrier diffusion length which can subsequently be mapped at the XRF beamline [7]. However, finding a direct correlation between recombination activity of a defect and its chemical nature was generally very difficult to achieve since it was almost impossible to match the maps obtained by independent $\mu$-XRF and lifetime measurement techniques with an accuracy of the order of a micron. Recently, we suggested a novel lifetime-sensitive technique, the x-ray-beam-induced current (XBIC) method [8]. The principle of the XBIC technique is similar to that of the EBIC or LBIC technique, the only difference being that minority charge carriers, generated by an electron beam in the EBIC or a laser beam in the LBIC, are generated in the XBIC by a focused x-ray beam. The electron beam or x-ray beam is scanned across the surface and the collected current is measured to form an image of the electrically active defects.

The XBIC signal, which carries information about the minority carrier lifetime, can be measured simultaneously with the $\mu$-XRF signal, which characterizes the chemical nature of the sample excited by the beam, including, e.g., impurity precipitates. This combination enabled us to study the chemical nature of the defects and impurities and their recombination activity *in situ* and to map metal clusters with a micron-scale resolution. In this study we report the application of XBIC/$\mu$-XRF techniques to the analysis of the recombination activity and space distribution of Cu and Fe in the vicinity of misfit dislocations in silicon/silicon–germanium structures.

## 2. Experimental technique and samples

The SiGe/Si structures each consisted of a 2 $\mu$m thick $Si_{0.98}Ge_{0.02}$ layer sandwiched between a 2.5 $\mu$m silicon bottom buffer layer on a (001) silicon substrate and a 2.5 $\mu$m thick silicon cap layer grown by chemical vapour deposition (CVD). All samples were phosphorus doped with a concentration of shallow donors of $10^{15}$ cm$^{-3}$. A network of two perpendicular sets of 60° misfit dislocations running in ⟨110⟩ directions was observed at the interfaces between silicon and silicon–germanium. The samples were intentionally contaminated with iron or copper by diffusion annealing at 1000 and at 800 °C, respectively. Additionally, one

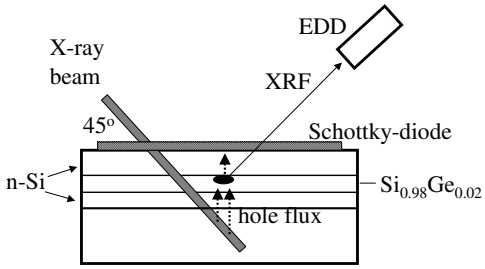


**Figure 1.** A schematic diagram of the XBIC/XRF experiment. The focused x-ray beam from a synchrotron is incident at an angle of 45° onto the sample surface. $\mu$-XRF arising when the beam hits the precipitate is measured by an Si:Li energy-dispersive detector (EDD). Minority carriers induced due to absorption of x-ray photons are collected with a Schottky diode. A reduction of the minority carrier diode current due to enhanced recombination at a defect gives rise to the appearance of the XBIC contrast.

iron-doped sample was treated in a remote hydrogen plasma reactor at 400 °C for 1 h, and another received the same thermal treatment in an inert ambient. Further details of the sample preparation can be found elsewhere [9, 10]. All samples investigated were pre-characterized using temperature-dependent EBIC. Some results of EBIC investigations of the samples can be found elsewhere [10].

To perform XBIC/$\mu$-XRF studies, 20 nm thick Pd or Au contacts were thermally evaporated on the surface of the chemically cleaned samples. The 20 nm layer of Pd or Au on top of the sample did not significantly absorb the x-rays, nor did it affect the penetration depth of the x-ray beam or the sensitivity of $\mu$-XRF technique.

Ohmic contacts were formed by rubbing gallium at the edges of the samples on the back surface. The sample was mounted in an XRF sample holder, which can be moved in the $X$-and $Y$-directions with a step size of 0.1 $\mu$m by computer-controlled step motors. The Schottky contact on the front of the sample and the ohmic contact on its back surface were contacted by thin palladium wires, which were connected to a sensitive current amplifier.

A diagram of the XBIC/$\mu$-XRF experiment is shown in figure 1. An intense x-ray beam from the synchrotron with approximately $3 \times 10^{10}$ photons $s^{-1}$ is focused into a 1–2 $\mu m^2$ spot using elliptically bent multilayer mirrors. The incident x-ray beam had a wide range of photon energies with a peak of intensity at 12.4 keV. The beam hits the sample surface at an angle of 45°. The emanating $\mu$-XRF is detected by a Si:Li detector with a resolution of about 180 eV. The penetration depth of the incoming x-rays is very large in silicon (about 250 $\mu$m). However, the sampling depth of the XRF technique is determined by the attenuation length of the fluorescence x-rays of interest (36 $\mu$m for iron and 70 $\mu$m for copper). The sensitivity of the XRF tool depends on the accumulation time, $t_a$, at each point. For $t_a = 30$ s a single iron precipitate with a radius of 20–25 nm, or dissolved iron or copper in concentration of about $10^{14}$ and $7 \times 10^{14}$ $cm^{-2}$ respectively can be detected [7]. The absolute values of the impurity concentration are determined using a calibration with XRF standards.

Due to the large attenuation depth of the exciting radiation, the XBIC sampling depth is determined primarily by the diffusion length of the excess minority carries. Additionally, the inclined beam orientation leads to a shift of the XBIC image with respect to the $\mu$-XRF in the direction of the beam projection on the sample surface. The excitation levels of the XBIC experiments are similar to those of a low-excitation regime for EBIC. Indeed, an x-ray photon flux of $10^{10}$ $cm^{-2}$ with an energy of 12.4 keV corresponds to the electron current of 1 nA. However, the absorbed energy is spread over a 250 $\mu$m x-ray penetration depth, which is

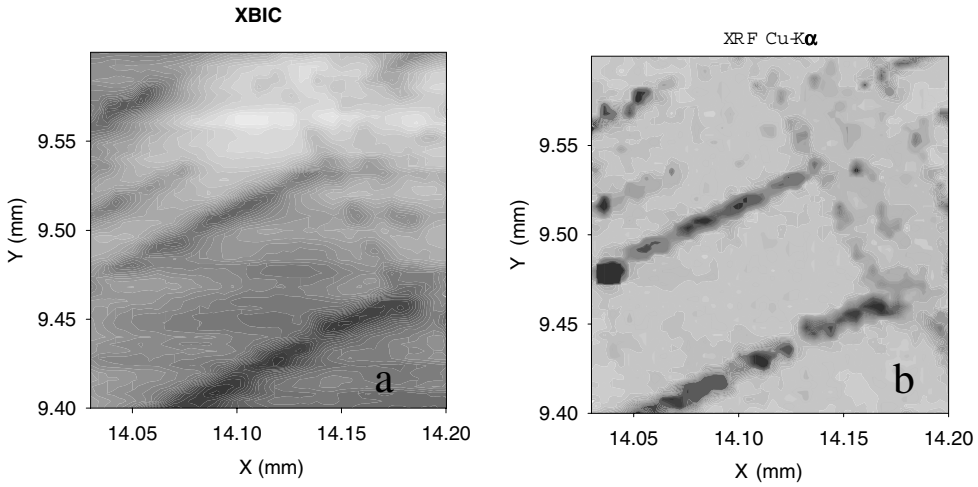


**Figure 2.** XBIC (left) and $\mu$-XRF maps of the Cu K$\alpha$ intensity distribution (right) of an area of a copper-doped Si–SiGe structure with misfit dislocations. Dark XBIC regions correspond to a reduction of the diode current whereas the dark Cu K$\alpha$ regions correspond to increased copper concentration. A good correlation between the recombination activity and the copper concentration distribution is obvious.

roughly 50 times greater than the penetration depth of the electrons of the same energy. Hence, the excitation conditions for an XBIC experiment correspond to approximately 20 pA electron beam excitation, i.e., a current which is considered to represent a low-excitation regime for EBIC.

No external bias was applied to the contact; the built-in voltage of the Schottky diode was used to collect the charge carriers. $\mu$-XRF and XBIC signals were measured simultaneously and were stored in a computer as a function of the $(X, Y)$ coordinates of the sample stage. These data could be later retrieved to plot the maps of minority carrier lifetime and metal impurity distribution, or to perform data analysis at any point within the scan.

## 3. Results and discussion

### *3.1. Copper-doped samples*

XBIC and XRF Cu K$\alpha$ maps of a SiGe/Si structure doped with copper are shown in figures 2(a) and (b), respectively. Dark areas on the XBIC map correspond to a reduction of the diode current, whereas the dark regions in the Cu K$\alpha$ map correspond to an increased copper concentration. One can see that the dark areas in both images are grouped in two sets of mutually perpendicular straight lines corresponding to two sets of misfit dislocations. Individual copper-rich precipitates can be distinguished in many parts of the XRF image. The XBIC image appears to be not very sharp due to the large generation volume of the exciting beam. There is however clearly a good correlation between the recombination activity and the copper concentration distributions, i.e., the higher the intensity of the copper-related $\mu$-XRF, the lower the XBIC.

Figure 3 shows an example of a quantitative treatment of the data presented in figure 2. It compares the profiles of the copper concentration and of the XBIC along the $x$-axis at $y = 9.4$ mm in figure 2. There is a good match between the copper distribution profile and the XBIC profile. In figure 4, the XBIC contrast is plotted against the copper concentration determined from the XRF maps. The XBIC contrast was calculated as the ratio $(I_0 - I_d)/I_0$,

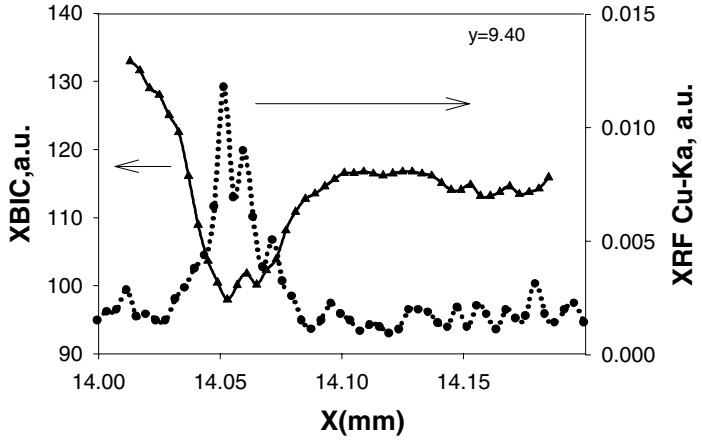


**Figure 3.** XBIC and $\mu$-XRF Cu K$\alpha$ linear scans across a copper-decorated misfit dislocation. The line scans are extracted from the maps in figure 2 along the horizontal axis at $y = 9.4$ mm.

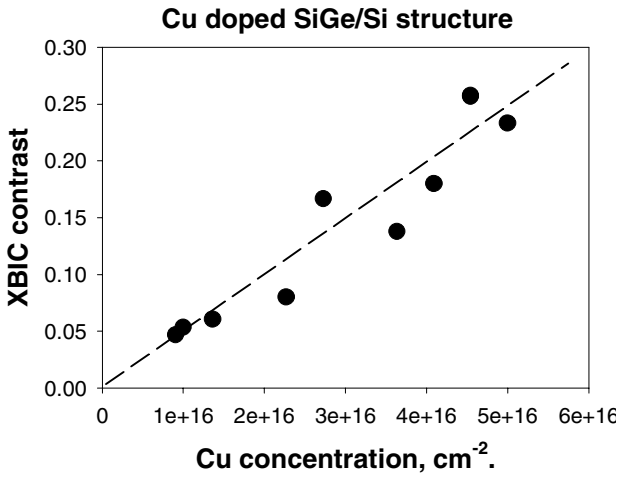


**Figure 4.** XBIC contrast versus XRF copper concentration as derived from multiple-line-scan data similar to those shown in figure 3. A linear dependence of the XBIC contrast on the Cu concentration is evident.

where $I_0$ is the XBIC value far away from the defect and $I_d$ is the value of the XBIC at the location of the precipitate. The maximum XBIC contrast value observed in our samples was about 30%, whereas the EBIC contrast for similar samples was up to 70%. Since the excitation levels of EBIC and XBIC are rather close to each other, we believe this discrepancy to be due to a smaller fraction of the total current being collected by the precipitates. Indeed, many of the carriers generated within a 250 $\mu$m path of the x-ray beam, penetrating into the sample at a 45° angle, will not be attracted by the space charge region around the metal precipitate and will diffuse straight to the Schottky diode.

An exact theory of the XBIC contrast with the particular generation function of the XBIC experiment does not exist at present. Nevertheless, the dependence of the contrast value on the recombination rate at extended defects must be close to a proportionality in any case [11]. Generally, the recombination rate depends on the electronic properties of a precipitate; those

in turn are dependent on its shape and size as well as on the origin of its electronic state. A phenomenological model of EBIC contrast due to sphere-shaped defects developed by Donolato [12] predicted the proportionality between the recombination strength of a defect and its radius in the limit of infinite recombination rate over the entire volume of the defect. In this case a sublinear power dependence of the recombination strength, $R_{e-h}$, on the defect volume, $V$, would be observed, $R_{e-h} \sim V^{1/3}$. On the other hand, the recombination at the surface of plate-like precipitates was suggested to be responsible for an extremely high recombination activity of the precipitates in silicon [13]. According to the models [6, 13], the recombination rate and the contrast must be proportional to the entire surface of the precipitates. A linear dependence of the recombination current on the number of atoms in the precipitate could then be observed when the thickness of the precipitates does not change significantly upon changes of their entire volume occurring.

To check whether this assumption is valid for our sample, we estimated an average thickness of the precipitates in the direction perpendicular to the sample surface from the absolute copper concentration determined from the XRF data, assuming that they consist of copper silicide, $Cu_3Si$, where the atomic density of Cu is $6 \times 10^{22}$ cm$^{-3}$ [14]. In this way, the average thickness of the precipitates observed in figure 3 was found to vary between 2 and 10 nm. These values are rather close to the minimum thickness of $Cu_3Si$ platelet-like precipitates found from TEM measurements for rapidly quenched samples as reported by Istratov *et al* [5]. If the variation of the real precipitate thickness were the only reason for the average thickness variation, then the XBIC contrast would be independent of the copper-atom density in the sample. Since we observed a linear dependence, it is likely that Cu precipitates are platelets of equal thicknesses but of different lateral sizes. Their true thickness cannot be extracted from our XRF data. More probably, they consist of precipitates of larger thickness than stated above and do not overlap significantly with each other.

### *3.2. Iron-doped samples*

XBIC maps of the Fe-doped samples showed strong contrast features corresponding to two perpendicular sets of misfit dislocations. The contrast consisted of straight lines with sharp edges running in ⟨110⟩ directions. Similar contrasts were observed in our EBIC experiments (not shown). A typical XBIC map of the samples is presented in figure 5(a). XRF measurements revealed the presence of Fe K$\alpha$ and Fe K$\beta$ peaks in the proper ratio confirming the presence of iron only in the sample that was treated in hydrogen plasma at 400 °C. The iron concentration in the reference sample, which was diffused with iron but not passivated in hydrogen plasma, was below the current detection limit of our set-up. For the hydrogen-passivated sample, the iron concentration was found to be rather homogeneously distributed within dislocation bunches and it was only 2–3 times larger than our detection limit (about $5 \times 10^{13}$ cm$^{-2}$). That is why we are not able to find a dependence of the XBIC contrast on the iron concentration like that presented for Cu in figure 4(b). A comparison of hydrogen-annealed and control Fe-contaminated samples suggested that some of the iron was gettered by the misfit dislocations during the hydrogen diffusion anneal (1 h at 400 °C). This shows that the impact of remote hydrogenation on minority carrier diffusion length cannot be described in terms of interaction of metals with hydrogen alone; it is a more complicated process.

Taking the distance between dislocations of 1 $\mu$m, we estimated the number of iron atoms per 1 cm length of dislocation from the iron concentration obtained from XRF measurement. This gives $10^{10}$ Fe cm$^{-1}$ which is two orders of magnitude larger than the linear atom density in silicon. This indicates that iron is probably included in clusters or microprecipitates along the dislocation line. In this case, the distance between the precipitates must be less than the

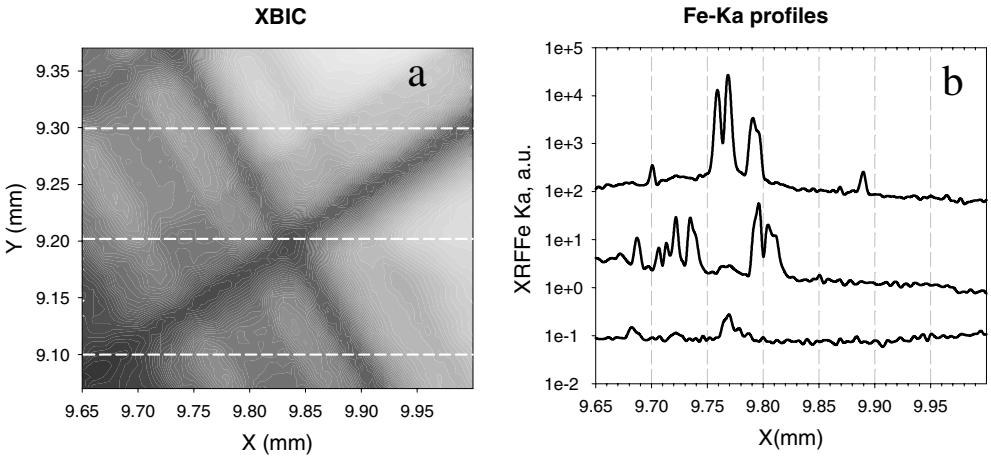


**Figure 5.** XBIC (left) and $\mu$-XRF maps of the Fe K$\alpha$ intensity distribution (right) of an iron-doped Si–SiGe structure with misfit dislocations. No direct correlation between the recombination activity and the iron concentration distribution was found.

spatial resolution of our measurement, which is about 2 $\mu$m. Assuming that the precipitates form iron silicide, $FeSi_2$, and taking its atomic density as $4 \times 10^{22}$ cm$^{-3}$, one can estimate the largest expected size of such a precipitate to be 30–40 nm.

To determine whether the separate precipitates could be detected, we performed line scans instead of two-dimensional mapping. Additionally, the acquisition time per point was significantly increased. In this way, a larger iron signal was found in some regions of the sample, indicating the presence of iron-containing precipitates. The results of that experiment are shown in figure 5(b), where three line scans of the Fe K$\alpha$ XRF peak were measured along the dashed lines drawn on the XBIC map (figure 5(a)). From the comparison of the XRF profiles (figure 5(b)) with the XBIC map (figure 5(a)), one can see that there is no one-to-one correlation between the positions and the magnitudes of XBIC and XRF signals. Precise examination of all available data revealed that large iron precipitates can frequently be found at the edges of dislocation bunches or at the intersections of the dislocations of two perpendicular sets. However, a higher iron concentration did not lead to any significant increase of the XBIC contrast. Assuming spherical precipitates, we could estimate the radius of the large inactive precipitates from the absolute iron concentration in the peaks of the XRF profiles (see figure 5(b)). In this way we obtained estimates for their sizes from 100 to 250 nm. Since this is a very large size, we think that most probably it is not the size of a single iron precipitate but rather that of clusters of precipitates each of a smaller size, as described above.

This estimate for the sizes of iron-containing precipitates is similar to that for copper-doped samples. Therefore, the spatial resolution of our XBIC measurements is not the reason that they are not seen. The only explanation is that iron precipitates are not electrically active. It is possible that the electrical inactivity of the iron precipitates is the result of the hydrogenation; however, additional experiments would be required to prove this hypothesis.

## 4. Conclusions

In summary, an analytical tool capable of *in situ* measurements of the recombination activity of defects and their chemical origin has been demonstrated in application to studies of copper-

and iron-contaminated misfit dislocations in silicon. A good correlation between the maps of the recombination activity and the density of the atoms in metal-containing precipitates was found. A proportionality between the XBIC contrast and the impurity atom density was found for copper-doped samples, whereas some large and electrically inactive precipitates were found in the Fe-doped sample treated in the hydrogen plasma.

## Acknowledgments

The funding for this research was provided by NREL, subcontract AAT-2-31605-03. The Advanced Light Source operations are funded by the Director, Office of Energy Research, Office of Basic Energy Sciences, Materials Sciences Division, of the US Department of Energy under Contract No DE-AC03-76SF00098. The authors gratefully acknowledge fruitful discussions with S A McHugo, H Hieslmair, G D Ackermann, R Ynzunza, and Z Hussain.

## References

[1] Istratov A A, Hieslmair H and Weber E R 2000 *Appl. Phys.* A **70** 489–534
[2] Istratov A A and Weber E R 1998 *Appl. Phys.* A **66** 123–36
[3] Riedel F, Kronewitz J, Gnauert U, Seibt M and Schröter W 1996 *Solid State Phenom.* **47–8** 359–64
[4] Riedel F and Schröter W 2000 *Phys. Rev.* B **62** 7150–6
[5] Istratov A A, Hedemann H, Seibt M, Vyvenko O F, Schröter W, Heiser T, Flink C, Hieslmair H and Weber E R 1998 *J. Electrochem. Soc.* **145** 3889–98
[6] Plekhanov P S and Tan T Y 2000 *Appl. Phys. Lett.* **76** 3777–9
[7] McHugo S A, Thompson A C, Flink C, Weber E R, Lamble G, Gunion B, MacDowell A, Celestre R, Padmore H A and Hussain Z 2000 *J. Cryst. Growth* **210** 395–400
[8] Vyvenko O F, Buonassisi T, Istratov A A, Hieslmair H, Thompson A C, Schindler R and Weber E R 2002 *J. Appl. Phys.* **91** 3614–17
[9] Kittler M, Seifert W and Higgs V 1993 *Phys. Status Solidi* a **137** 327–35
[10] Kittler M, Ulhaq-Bouillet C and Higgs V 1995 *J. Appl. Phys.* **78** 4573–83
[11] Donolato C 1992 *Semicond. Sci. Technol.* **7** 37–43
[12] Donolato C 1993 *Semicond. Sci. Technol.* **8** 45–9
[13] Kittler M, Larz J, Seifert W, Seibt M and Schröter W 1991 *Appl. Phys. Lett.* **58** 911–13
[14] Ronay M and Schad R G 1990 *Phys. Rev. Lett.* **64** 2042–5